

Segmentation-based blood flow parameter refinement in cerebrovascular structures using 4D arterial spin labeling MRA

R. Phellan*, T. Lindner, M. Helle, A. X. Falcão, C. L. Yasuda, M. Sokolska, R. H. Jäger, N. D. Forkert

Abstract—Objective: Cerebrovascular diseases are one of the main global causes of death and disability in the adult population. The preferred imaging modality for the diagnostic routine is digital subtraction angiography, an invasive modality. Time-resolved three-dimensional arterial spin labeling magnetic resonance angiography (4D ASL MRA) is an alternative non-invasive modality, which captures morphological and blood flow data of the cerebrovascular system, with high spatial and temporal resolution. This work proposes advanced medical image processing methods that extract the anatomical and hemodynamic information contained in 4D ASL MRA datasets. **Methods:** A previously published segmentation method, which uses blood flow data to improve its accuracy, is extended to estimate blood flow parameters by fitting a mathematical model to the measured vascular signal. The estimated values are then refined using regression techniques within the cerebrovascular segmentation. The proposed method was evaluated using fifteen 4D ASL MRA phantoms, with ground-truth morphological and hemodynamic data, fifteen 4D ASL MRA datasets acquired from healthy volunteers, and two 4D ASL MRA datasets from patients with a stenosis. **Results:** The proposed method reached an average Dice similarity coefficient of 0.957 and 0.938 in the phantom and real dataset segmentation evaluations, respectively. The estimated blood flow parameter values are more similar to the ground-truth values after the refinement step, when using phantoms. A qualitative analysis showed that the refined blood flow estimation is more realistic compared to the raw hemodynamic parameters. **Conclusion:** The proposed method can provide accurate segmentations and blood flow parameter estimations in the cerebrovascular system using 4D ASL MRA datasets. **Significance:** The information obtained with the proposed method can help clinicians and researchers to study the cerebrovascular system non-invasively.

Index Terms—Angiography, vascular segmentation, hemodynamic analysis, magnetic resonance angiography.

Manuscript October 30, 2019. Asterisk indicates corresponding author.

R. Phellan and N. D. Forkert are with Department of Radiology and Hotchkiss Brain Institute, University of Calgary, 3330 Hospital Drive NW, Calgary, AB, Canada (e-mail: phellan.renzo@ucalgary.ca). T. Lindner is with Department of Radiology, University Hospital Hamburg-Eppendorf, Hamburg, Germany. M. Helle is with Philips Technologie GmbH, Innovative Technologies, Hamburg, Germany. C. L. Yasuda is with Department of Neurology, Faculty of Medical Sciences, University of Campinas, Campinas, SP, Brazil. A. X. Falcão is with Laboratory of Image Data Science, Institute of Computing, University of Campinas, Campinas, SP, Brazil. M. Sokolska is with University College London Hospitals NHS Foundation Trust, London, United Kingdom. R. H. Jäger is with Neuroradiological Academic Unit, UCL Institute of Neurology, Queen Square, London, United Kingdom

Copyright (c) 2019 IEEE. Personal use of this material is permitted. However, permission to use this material for any other purposes must be obtained from the IEEE by sending an email to pubs-permissions@ieee.org

I. INTRODUCTION

Cerebrovascular diseases are one of the main global causes of death and disability in the adult population [1]. Currently, the preferred medical imaging modality used to diagnose, study, and plan how to treat these diseases is X-ray digital subtraction angiography (DSA) as it can be acquired with high temporal resolution, which is needed for the analysis of cerebral blood flow dynamics [2]. Nevertheless, due to its invasive nature during the catheterization process, administration of a contrast agent, and the exposure of the patient to ionizing radiation, DSA is associated with various complications, such as reversible or permanent neurologic deficits, thromboembolism, arterial dissection, allergic reactions to contrast agent, and increased risk of cancer [3]. It is important to mention that the probability of occurrence of those complications is below six percent according to different studies [3], [4]. However, their undesirable effects turn them into a considerable risk that should be avoided, if possible. Moreover, DSA is essentially a bi-dimensional projection technique, which might miss important anatomical information, noticeable in three dimensions.

An emerging non-invasive alternative to DSA is time-resolved three-dimensional (i.e. 4D) arterial spin labeling magnetic resonance angiography (ASL MRA) [2]. 4D ASL MRA is less invasive than DSA because it uses MR imaging to magnetically label the patient's blood as an intrinsic contrast agent flowing through the brain. Thus, no ionizing radiation, catheterization, or administration of an external contrast media is required. Additionally, 4D ASL MRA can simultaneously capture blood flow and morphological data of the cerebrovascular system, which is not possible with other commonly used imaging modalities, such as time-of-flight magnetic resonance angiography (TOF MRA). Finally, 4D ASL MRA is capable of achieving higher spatial and temporal resolution [2] when compared to other common contrast agent-based 4D MRA modalities, such as 4D Time-Resolved MRA with Keyhole (4D-TRAK) [5], Time-Resolved Imaging of Contrast Kinetics (TRICKS) [6], and Time-resolved Angiography with Interleaved Stochastic Trajectories (TWIST) [7].

However, 4D ASL MRA generates a considerable amount of data, which is tedious to analyze by direct visual analysis. In this case, medical image processing methods can be used to extract the morphological and blood flow data contained in 4D ASL MRA datasets and present it in a more useful format to clinicians and researchers. For example, the information can be presented as geometric measurements of the density, tortuosity,

and thickness of vessels, globally as well as regionally, or as color-coded three-dimensional visualizations of the relative blood volume A , transit time δ_t , blood dispersion sharpness s , and time-to-peak p along the vessels (see Figure 1). These measurements and visualizations have proven to be useful for clinical and research purposes [8]–[10].

Many different vascular segmentation methods have been developed to extract the morphological data contained in medical images [11]. However, only a few of them take advantage of both, morphological and blood flow data, in order to increase the accuracy of the final result. Deschamps et al. [12] developed a level-set method for segmentation of the brain vessels from 3D MRA datasets, whereas the resulting segmentation was then used as the basis for blood flow simulation. Mordang et al. [13] developed a method for the analysis of 4D computed tomography angiography (CTA datasets), acquired after the administration of a contrast agent to the patient. Their method extracts a set of features for each voxel of the series of images, and uses those features to train a linear discriminant classifier able to differentiate between vessels and other tissues present in the medical images. Pathwardan et al. [14] proposed a 4D vessel segmentation for ultrasound images. The algorithm requires an initial seed point inside the vessel, which is manually defined. The initial seed point is used to detect and track the vessel centerline in a time sequence of 3D ultrasound images. Once the centerline is identified, an active contour model is used to track the vessel surface. 4D flow MRI is another medical imaging modality, with a spatial resolution similar to 4D ASL MRA, that captures morphological and blood flow data of the cerebrovascular system [15], [16]. Dunås et al. [15] recently optimized and evaluated three different methods to extract the vascular system from this image modality based on k-means clustering, and global and local thresholding to identify major cerebral arteries, which are then used to measure the blood flow velocity. In contrast to 4D ASL MRA, 4D flow MRI does not display the passage of a magnetically labeled bolus through vessels but measures the blood flow velocity at different stages of the cardiac cycle directly. Finally, Phellan et al. [17] developed a segmentation method, without an explicit hemodynamic analysis, specifically designed for vascular segmentation of 4D ASL MRA, which reaches considerable high accuracies by using both, morphological and blood flow data. It is important to note that in all cases described above, the hemodynamic analysis is applied to each voxel containing vascular signal in an isolated manner, consequently neglecting the spatial dependency of blood flow parameters, which is important because the blood flow is not expected to change dramatically for neighbouring voxels. However, the spatial information provided by the vascular segmentation can be used to refine and improve the hemodynamic analysis.

The objective of this work is to extend the cerebrovascular segmentation method developed by Phellan et al. [17], to extract and refine the hemodynamic parameters included in 4D ASL MRA datasets. More precisely, the morphological data is used to refine the estimated blood flow parameter values, considering their spatial dependency. This new method would allow clinicians and researchers to fully leverage the data con-

tained in 4D ASL MRA datasets to study the cerebrovascular system in a non-invasive way.

II. MATERIALS

Fifteen 4D ASL MRA datasets from healthy volunteers are used in this work. The datasets were acquired with approval of a local institutional ethics committee (Ärztchamber Schleswig-Holstein and Calgary Health Regional Ethic Board) and all subjects provided written informed consent consistent with the Declaration of Helsinki to participate in this study. Each 4D ASL MRA dataset was acquired as a set of six control/labeled volumetric image pairs, with a temporal resolution of 120 *ms*, on a Philips Achieva 3T MRI device (Philips Healthcare, Best, The Netherlands). Blood was magnetically labeled for 300 *ms* using pseudo-continuous arterial spin labeling (PCASL) [18] and a delay of 20 *ms* was used before starting the image acquisition. Each volumetric image in a 4D ASL MRA dataset has a voxel size of $0.94 \times 0.94 \times 1.0 \text{ mm}^3$ and contains 120 slices, with 224×224 voxels. Additional image acquisition parameters include: T1-Turbo Field Echo (TFE) scan with a TFE factor of 16, SENSitivity Encoding (SENSE) factor: 3, TR/TE: 7.7/3.7 *ms*, flip angle: 10° , half scan factor: 0.7. The total acquisition time of a dataset was 5 minutes.

In order to obtain reference cerebrovascular segmentations for the 4D ASL MRA datasets, time-of-flight magnetic resonance angiography (TOF MRA) volumetric images were also acquired from the same fifteen volunteers. The size of the TOF MRA 3D images is 171 slices with 512×512 voxels and voxel size $0.41 \times 0.41 \times 0.70 \text{ mm}^3$. Other image acquisition parameters include: SENSE factor: 2, TR/TE: 20/3.45 *ms*, flip angle: 20° , 3 slabs, and flow compensated readout. The total acquisition time was 6:40 minutes.

Additionally, two 4D ASL MRA datasets from patients with a stenosis in the carotid arteries are included in the experiments as a proof-of-principle that the proposed method can be applied to datasets of patients with a vascular pathology. The datasets were acquired with approval of the local institutional ethics committee and all subjects provided written informed consent consistent with the Declaration of Helsinki. In this case, the 4D ASL MRA datasets contain ten control/labeled volumetric image pairs, acquired with a temporal resolution of 120 *ms* using a Philips Achieva 3T MRI device (Philips Healthcare, Best, The Netherlands). A pulsed arterial spin labeling (PASL) [19] acquisition method was used and a delay of 60 *ms* was employed before starting the image acquisition. Each volumetric image in these 4D ASL MRA datasets consists of 75 slices with 256×256 voxels, exhibiting a spatial resolution of $0.82 \times 0.82 \times 0.8 \text{ mm}^3$. Additional image acquisition parameters include: Turbo-Field Echo Planar Imaging (TFEPI) scan with a TFE/EPI factor of 7/7, SENSE factor: 2.5, TR/TE: 13/4.7 *ms*, flip angle: 10° . The total acquisition time of a dataset was 2:07 minutes.

III. METHODS

The pipeline of the proposed segmentation-based hemodynamic analysis and refinement method is presented in Figure 1. Each step is described in the following subsections.

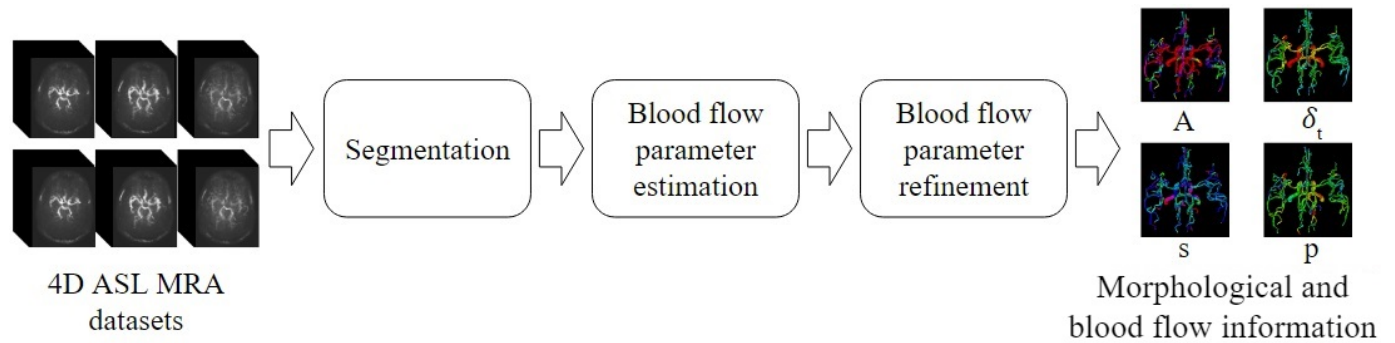


Fig. 1. Pipeline of the proposed segmentation-based blood flow parameter refinement method. The input of the pipeline is a 4D ASL MRA dataset and the output is the segmented cerebrovascular system with estimated blood flow parameters: relative blood volume A , transit time δ_t , blood dispersion sharpness s , and time-to-peak p along the vessels.

A. Segmentation

In the first step of the proposed method, the vascular system is extracted from the 4D ASL MRA dataset using the method described in [17], which is summarized in the following. This method starts by filtering each control/labeled pair of a 4D ASL MRA dataset using a denoising algorithm [20] to reduce the noise, without blurring edges and thin vascular structures. The labeled image is then subtracted from the control image to remove the signal of non-vascular tissues, but some residual noise can still be observed, even after subtraction, particularly in the last images of the 4D ASL MRA sequence. As a last preprocessing step, the subtracted images are filtered using the multiscale vesselness filter designed by Erdt et al. [21], which enhances the intensity of vessels in the images and has been shown to help to increase the accuracy of the final segmentation [22].

After pair-wise subtraction of the control and label images, followed by vessel enhancement filtering, the first two images of the 4D ASL MRA datasets usually contain only large vessels, with high vascular signal intensities and low background noise. Therefore, a simple k-means algorithm is used to extract the arteries from the first two timepoints. These initial segmentations are refined using a level-set segmentation algorithm in order to include possible missing voxels that contain vascular signal. Therefore, the level-set approach proposed by Lankton et al. [23] is used, which considers neighboring voxels within a sphere of a predefined radius to be added or removed from the initial segmentation depending on whether they increase or reduce the inter-class distance between vascular and non-vascular tissues. After vessel segmentation in the first two images of a 4D ASL MRA dataset, the two corresponding segmentations are combined using an *OR* operator.

Starting with the third image of a 4D ASL MRA dataset, the signal of magnetically labeled blood tends to be considerably affected by phenomena such as dispersion of labeled blood and magnetic signal decay. These phenomena lead to artifacts in the k-means segmentation, such as gaps with low intensity values in the middle of vessels, and reduce the signal of small vessels to values similar to noise. Consequently, additional sophisticated segmentation strategies are required to segment the later timepoints of a 4D ASL MRA dataset.

As described in [17], the image foresting transform (IFT)

algorithm [24] is used to fill the gaps present in the k-means vessel segmentation results of the later time points. The IFT algorithm is particularly useful for this application, because it can always find an optimal path between two disconnected segments of a vessel, according to a connectivity function. The function can be modeled so that the optimal connecting path contains neighboring voxels with the highest signal intensity. Here, it is assumed that the optimal path with the highest average signal intensity is the most reasonable choice to connect two segments of the same vessel. The thickness of the optimal connecting path is calculated by linear interpolation between the values of the thickness of the segments it connects.

Additionally, the reduced signal of small vessels, with values similar to noise, can considerably affect the initial segmentation obtained using the k-means algorithm. The first strategy to overcome this problem is to refine the initial segmentation with the same level-set segmentation algorithm used to refine the segmentation of the first two frames of the dataset [23]. The second strategy to remove noise adjacent to vascular structures, with similar intensity values, is to continuously follow magnetically labeled blood as it flows through the arteries. In particular, only new segmented sections of the cerebrovascular system visible at one timepoint that are connected to arteries already segmented in the two previous timepoints are added to the final segmentation.

B. Blood flow parameter estimation

After the vascular system is segmented in a 4D ASL MRA dataset, an hemodynamic analysis is performed to calculate relevant blood flow parameters. This hemodynamic analysis is essentially restricted to vessels segmented in the previous step. Considering that 4D ASL MRA provides only discrete values of the signal evolution curve of a voxel with a fixed temporal resolution, a continuously defined mathematical model is fitted to the discrete time curve, which enables the calculation of hemodynamic parameters with higher accuracy. Additionally, fitting a mathematical model helps to mitigate the influence of noise in the estimation of blood flow parameters [25].

The mathematical model selected for the purpose in this work was specifically designed to describe the concentration time curve in 4D ASL MRA images [26]. It is the only model available for this modality that considers blood flow

of magnetically labeled blood through the arteries of the cerebrovascular system, before reaching capillaries that are responsible for perfusion of the brain tissue. The mathematical function of the model is shown in Equation 1.

$$S(v, t) = \int_{t-\delta_t-\tau}^{t-\delta_t} A(v)D(v, t_d)T(\delta_t, t_d)R(t)dt_d \quad (1)$$

$$D(v, t_d) = \begin{cases} \frac{s}{\Gamma(1+ps)e^{st_d}}(st_d)^{ps} & \text{if } st_d > 0, ps > -1 \\ 0 & \text{otherwise} \end{cases} \quad (2)$$

$$T(\delta_t, t_d) = e^{-(\delta_t+t_d)/T_{1b}} \quad (3)$$

$$R(t) = \cos(\alpha)^{(t-t_0)/TR} \sin(\alpha) \quad (4)$$

In this model, the 4D ASL MRA signal $S(v, t)$ of a voxel v at timepoint t depends on four main phenomena, which comprise the relative volume of magnetically labeled blood flowing through that voxel $A(v)$, the dispersion $D(v, t_d)$ that labeled blood experiences before reaching the voxel v , the signal attenuation $T(\delta_t, t_d)$ due to T_1 decay of the magnetic label, and the signal attenuation $R(t)$ caused by the imaging radiofrequency pulses applied to the labeled blood in previous timepoints. Additionally, $S(v, t)$ depends on the blood transit time δ_t from the labeling plane to voxel v and the duration used to magnetically label blood τ .

Each of the previously mentioned phenomena depends on additional parameters, described in the following. First, the dispersion of blood $D(v, t_d)$ is modeled by a distribution defined by the blood flow parameters s and p (see Equation 2), which control the distribution's sharpness and time to peak, respectively, normalized using the gamma function (Γ). The signal attenuation due to T_1 decay $T(\delta_t, t_d)$, defined in Equation 3, requires the parameter T_{1b} , which represents the longitudinal relaxation time of arterial blood. The value of T_{1b} at 3T is 1664 ± 14 ms, according to Lu et al. [27]. Finally, in the term $R(t)$ (see Equation 4), the parameter α corresponds to the flip angle used to acquire the 4D ASL MRA dataset, t_0 is the time at which the first imaging pulse is applied, and TR is the repetition time. The model assumes that all transverse magnetization is spoiled at the end of every TR , so that the longitudinal magnetization is reduced by a factor of $\cos(\alpha)$ with every pulse. The factor $\sin(\alpha)$ accounts for the amount of transverse magnetization generated from a given longitudinal magnetization. In this work, the simplified version of the term $R(t)$, proposed by Okell et al. [26], is used assuming that the imaging region comprises only anatomical structures distal to the labeling plane, which is a reasonable assumption for brain arteries.

Most of the parameters required in the blood flow model are acquisition parameters and their values can be obtained directly from the 4D ASL MRA imaging protocol. However, the blood flow parameters $A(v)$, δ_t , s , and p have to be estimated using the signal of magnetically labeled blood flowing through the cerebrovascular system over time acquired in a 4D ASL MRA dataset.

The multi-scale parameter search (MSPS) algorithm is used in this work to fit the mathematical model described above to the discrete 4D ASL MRA signal curve of each voxel in the segmented vascular system as it ranks well in different

benchmarks when compared to other algorithms designed for parameter optimization [28]. The metric used for optimization by the MSPS algorithm is to minimize the average absolute error (AAE) between the observed 4D ASL MRA signal in a voxel and corresponding values of the fitted hemodynamic model as defined by the optimization parameters in each iteration. The AAE was selected instead of the sum of squared differences because it was observed that the fitting error could lead to values considerably smaller than 1. When squared, those values may be too small to be represented accurately in the hardware used for the experiments, which could misguide the exhaustive search.

C. Blood flow parameter refinement

At this stage, each 4D ASL MRA dataset is segmented and the blood flow parameters $A(v)$, δ_t , s , and p have been calculated for every voxel included in each binary segmentation of the cerebrovascular system. However, the extracted blood flow parameters show many physiologically impossible discontinuities along the vessel (see top row of Figure 2), which is not only a result of noise, but also a result of the independent analysis of each voxel. In order to mitigate this problem, it is proposed in this work to apply advanced heuristics in a post-processing step.

Therefore, the blood flow data estimated in the binary segmentations of 4D ASL MRA datasets of healthy subjects was analyzed in order to identify patterns that can be used to define heuristics. More precisely, the binary segmentations were skeletonized using an algorithm available as an extension to the Insight Toolkit (ITK) [29], [30], because the most relevant blood flow information in 4D ASL MRA datasets is located along the centerline of the cerebrovascular system [8]. The selected algorithm has been successfully used to skeletonize the hepatic vasculature in various datasets, without creating any disconnected regions and locating the skeleton lines in the center of the structure.

There are three main arteries that supply blood to the brain: the left and right internal carotid arteries (LICA and RICA), and the basilar artery (BA). For each of these arteries, the longest main artery path within the skeletonized segmentation, considering all vessel ends in the skeletonized segmentation, is identified using the image foresting transform (IFT) algorithm [24].

The IFT interprets the skeleton of the vascular system as a weighted graph, where every voxel represents a vertex and an edge is drawn between any two neighboring vertices, considering a 26-neighborhood. The weight $W(u, v)$ assigned to any edge is the physical distance between its vertices, the voxels u and v . Then, the function l , defined in Equation 5, is used to assign a value $l(\pi_v)$ to any path π_v in the graph, which represents the total length of the path. The IFT algorithm considers two types of paths during its execution: trivial paths consisting of a single voxel $\pi_v = \langle v \rangle$ and non-trivial paths with more than one voxel $\pi_v = \langle v_1, v_2, \dots, v_n = v \rangle$. Additionally, the IFT requires a set of seed voxels $v \in S$ that define one of the extremes of any path. In this case, each final section of an artery is considered in the set. The seed voxels can be

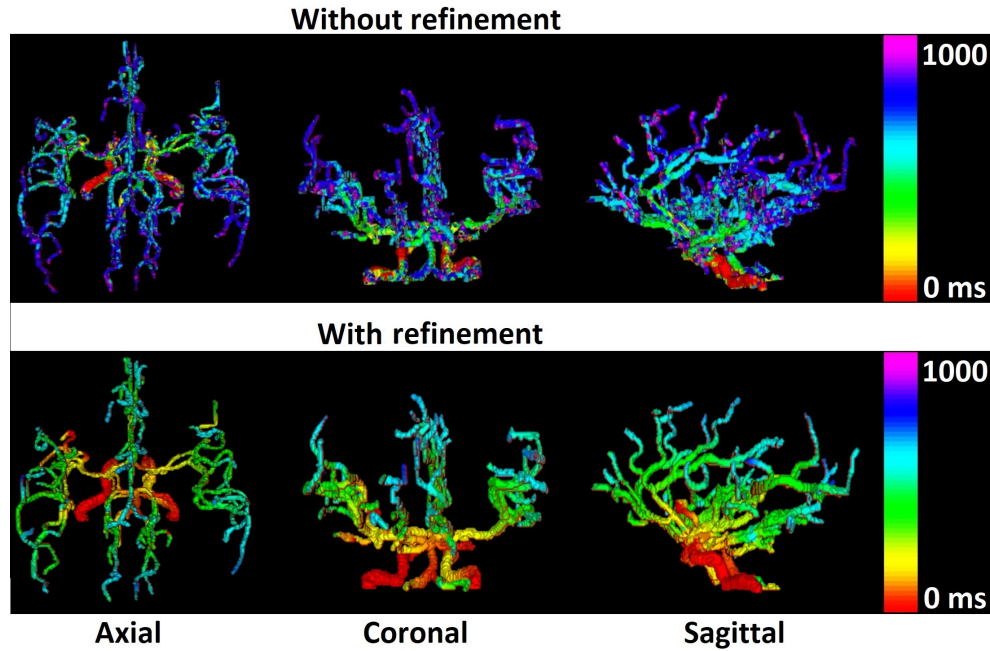


Fig. 2. Axial, coronal, and sagittal bi-dimensional views of the values estimated for the parameter δ_t , without and with the refinement step.

automatically identified as the voxels in the skeleton with only one adjacent neighbor, considering a 26-neighborhood.

$$\begin{aligned}
 l(\langle v \rangle) &= \begin{cases} 0 & \text{if } v \in S, \\ -\infty & \text{otherwise,} \end{cases} \\
 l(\pi_u \cdot \langle u, v \rangle) &= l(\pi_u) + W(u, v). \quad (5)
 \end{aligned}$$

The IFT algorithm starts by assigning trivial paths to all vertices. Then, in each iteration, a vertex u with minimum path length $l(\pi_u)$ is found and offers extended paths $\pi_u \cdot \langle u, v \rangle$ to its adjacent nodes v . As the objective of this algorithm is to maximize the average path length of all paths, if $l(\pi_u \cdot \langle u, v \rangle) > l(\pi_v)$, the algorithm substitutes π_v by the extended path $\pi_u \cdot \langle u, v \rangle$. The number of iterations the IFT algorithm requires is equal to the number of vertices in the skeleton and it outputs an optimal set of paths of maximum length.

Once the skeletonized cerebrovascular system is split into paths of maximum length, the estimated blood flow parameter values of the voxels along each path, in relation to the distance from the main artery seeds, were plotted and visually analyzed for all healthy subjects. Here, it was noticed that the transit time δ_t , sharpness s , and time-to-peak p of the distribution that models the blood flow dispersion follow an approximately linear distribution, with respect to its trajectory along the vascular tree, starting at the labeling plane. The relative blood volume A , however, appears to be better approximated by a quadratic distribution. This can be explained by the fact that A is proportional to the cross-sectional area of the vessel that contains the voxel analyzed. This area is proportional to the square of its radius and the radius follows an approximately linear distribution along the vascular tree. Based on the identified patterns, a regression analysis was performed for each longest path.

Figure 3 shows the plotted values of each blood flow

parameter along the centerline of the path of maximum length in the skeleton of one selected segmented cerebrovascular system, which shows a linear pattern in case of the transit time δ_t , sharpness s , and time-to-peak p , and the quadratic pattern of the relative blood volume A .

Table I shows the average and range of the correlation values (r) when applying the corresponding regression analysis comparing each blood flow parameter estimated to the corresponding vessel distance in the fifteen 4D ASL MRA datasets from healthy volunteers used in this work. The average value of r was calculated using the method proposed by Corey et al. [31], which was proven to be a less biased estimate of the population correlation coefficient when correlation coefficients from a small sample are averaged. The average r is greater or equal than 0.7 in all cases, which suggests a strong correlation of the corresponding model, either linear or quadratic. Despite the fact that the datasets share similar patterns for each blood flow parameter, either linear or quadratic, does not imply that the regression coefficients and constants are the same across subjects.

Parameter	r average and range
A	0.846 [0.683, 0.925]
δ_t	0.863 [0.748, 0.949]
s	0.700 [0.578, 0.824]
p	0.736 [0.648, 0.808]

TABLE I
CORRELATION COEFFICIENT (r) AVERAGE AND RANGE FOR EACH ESTIMATED BLOOD FLOW PARAMETER VALUE IN RELATION TO THE VESSEL DISTANCE, OBTAINED WHEN APPLYING REGRESSION ANALYSIS TO THE FIFTEEN 4D ASL MRA DATASETS FROM HEALTHY VOLUNTEERS ACQUIRED FOR THIS WORK.

Based on the findings described above, the proposed refinement of the blood flow parameter values estimated in the cerebrovascular system starts with the skeletonization and sub-

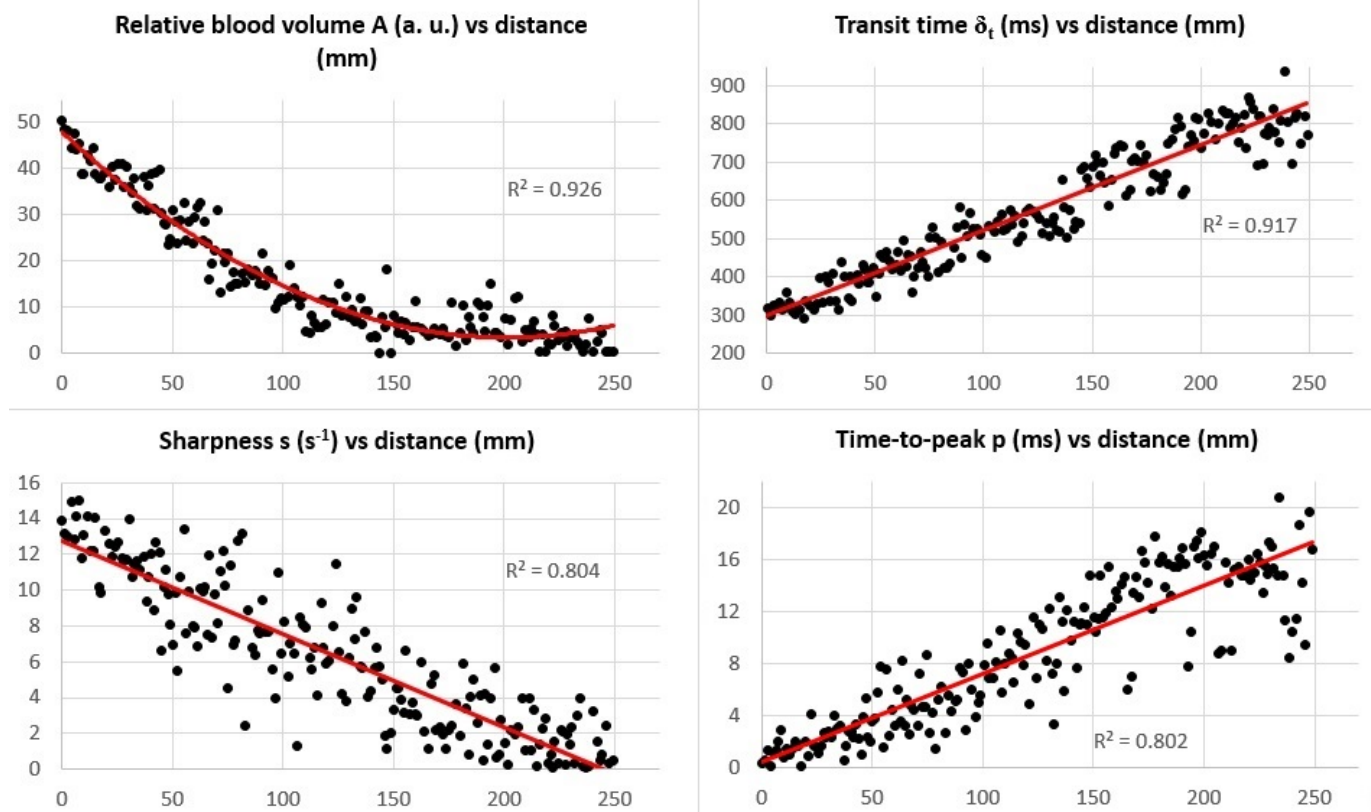


Fig. 3. Plotted values of each blood flow parameter (relative blood volume A , transit time δ_t , sharpness s , and time-to-peak p of the distribution that models the blood flow dispersion) along the centerline of the path of maximum length in the entire skeleton of a segmented cerebrovascular system, as a function of the distance from the seed of the corresponding main feeding artery.

division into maximum length paths of the binary segmentation. Then, the values of δ_t , s , and p along the skeleton are refined using a linear regression, while the values of A are approximated with a quadratic polynomial as a function of the distance from the seed of the corresponding main feeding artery. The refinement of the blood flow parameters is performed iteratively starting with the longest path identified in each skeleton until reaching the shortest one. The reason to start with the longest paths is that they contain the largest number of voxels with data, which is expected to lead to a better fit of the regression function. In case a path is connected to a longer path, the regression is restricted to fit to the value of the longest path at the bifurcation under the assumption that initial refinements lead to a better fit with more available data. Finally, the values of each voxel of the skeleton are copied back to the initial segmentation by considering the Voronoi region of influence. It is expected that this refinement reduces the AAE between the estimated and ground-truth blood flow parameter values.

D. Evaluation method

In this work, the proposed hemodynamic refinement method is evaluated in three different scenarios. First, virtual 4D ASL MRA phantoms with ground-truth binary segmentations and blood flow parameter values are used for quantitative evaluation of the segmentation results and hemodynamic analysis, before and after the blood flow parameter refinement

step. Second, real 4D ASL MRA datasets are also used for quantitative evaluation of the segmentation results but the hemodynamic refinement method is evaluated qualitatively by a neurologist as no ground-truth blood flow parameter values are available in this scenario. Third, the results of applying the proposed hemodynamic refinement method to 4D ASL MRA datasets of patients with a stenosis in the carotid arteries are also included and discussed in this work.

The 4D ASL MRA phantoms were generated using the methodology proposed by Phellan et al. [32], briefly described in the following. First, an automatic and validated method [33] is used to segment the vessels in the TOF MRA images, which present higher spatial resolution than 4D ASL MRA images, but contain no hemodynamic data. Then, blood flow parameter values are assigned to each voxel in this high resolution space according to flow patterns and blood flow measurements derived from healthy subjects [34], [35]. Next, the same formula used for the blood flow parameter estimation described in Section III-B (see Equation 1) is used to generate a 4D ASL MRA phantom with a time series of images in TOF MRA space. After that, the hemodynamic parameter images and corresponding 4D ASL MRA images are downsampled to 4D ASL MRA space using linear interpolation. In doing so, partial volume effects are added to the simulated 4D ASL MRA datasets. The ground-truth binary segmentations of the cerebrovascular system in 4D ASL MRA space are generated by thresholding a temporal maximum intensity projection of

the corresponding resampled 4D ASL MRA images, using a low threshold value, such as 0.0001. Finally, noise is added to the phantoms following an homomorphic approach [36], which can accurately replicate the noise with local image variation that results as a consequence of multi-coil acquisitions, such as 4D ASL MRA.

For quantitative evaluation of the segmentation results using the annotated phantoms and the real 4D ASL MRA datasets, the accuracy of the vascular segmentation is measured using the Dice similarity coefficient (DSC), defined in equation 6, in terms of the number of true positives (TP), false positives (FP), and false negatives (FN). The DSC [37] measures the overlap between the ground-truth and automatically extracted segmentations, and it is commonly used for evaluation of the segmentation of thin structures [11]. However, the DSC penalizes even slight differences between voxels at the border of the structures, which represent a small percentage of the total score in the case of blob-like structures but a considerable percentage in case of thin structures, such as vessels. In order to compensate for this penalization, a tolerance margin of one voxel was added to the computation of the DSC. The tolerance margin is implemented by dilating and eroding the ground-truth and reference segmentation using a spherical structuring element with a radius of 1 voxel. False positives inside the dilated region are counted as true positives and false negatives outside the eroded region are counted as true negatives.

$$DSC = \frac{2TP}{2TP + FP + FN} \quad (6)$$

It should be noted that, in case of the real 4D ASL MRA datasets, the calculated segmentations are compared to reference segmentations obtained by an automatic validated method in TOF MRA images [33] with higher spatial resolution but not containing blood flow data. In order to transform the TOF MRA segmentations into 4D ASL MRA space, each volumetric TOF MRA image is registered to a temporal maximum intensity projection of the corresponding 4D ASL MRA dataset of the same subject using the Elastix software [38], configured for rigid transformation, b-spline interpolation, and mutual information as similarity criterion. After that, the obtained transformation is applied to the TOF MRA binary vessel segmentation using a nearest-neighbor interpolation. The reference segmentations, in 4D ASL MRA space, were revised and manually corrected to mitigate possible errors, if necessary.

The blood flow parameter values estimated for the phantoms and their corresponding ground-truth are compared using the AAE metric, which was also used to guide the MSPS search used to optimize the fitting of the hemodynamic model function for the blood flow parameter estimation. The AAE was determined to be normally distributed, according to a Kolmogorov-Smirnov test of normality. Consequently, in order to evaluate the improvement in terms of AAE obtained with the blood flow refinement step, a standard one-way analysis of variance (ANOVA), followed by the Tukey's honest significant difference procedure is used to test for significant differences between the AAE of each estimated blood flow parameter

($A(v)$, δ_t , s , and p), before and after refinement. The Statistical Package for the Social Sciences version 16.0 (SPSS Inc., Chicago, IL, USA) was used for the statistical analysis, and the criterion of statistical significance was set at p-value < 0.05.

The qualitative evaluation of the estimated blood flow parameters, using the real clinical datasets, was performed by a neurologist with more than 20 years of experience working in brain image analysis. In a first step, the neurologist reviewed 15 image sequences, each containing renderings of the color-coded surface visualizations of the relative blood volume and transit time hemodynamic parameters from the three orthogonal views (axial, coronal, and sagittal). For each subject dataset, the raw or refined hemodynamic parameters (see Figure 2) were randomly selected for the qualitative analysis of the visualization. Then, 30 days later, the neurologist performed the same qualitative evaluation again, but using the raw or refined hemodynamic parameter versions of the visualizations not used in the first evaluation. In doing so, the visualization using the raw and refined hemodynamic parameters were qualitatively evaluated for each subject, thus allowing a comparison of both. The 30 days break between the rating was used to prevent a potential memory bias.

For qualitative evaluation, the medical expert was asked to rate every visualization based on the three orthogonal views regarding the physiological plausibility on a scale from 0 to 6. Here, 0 indicates that a visualization is not plausible regarding the expected hemodynamic physiology, while 6 indicates high plausibility. The blood volume and transit time parameters were used for this evaluation only as these are considered important parameters for the analysis of the cerebrovascular system [39], while the sharpness and time-to-peak are considered less intuitive for this hemodynamic model. Regarding the datasets of patients with a stenosis, a visual assessment was used to evaluate if the proposed method can be used in patients with vascular pathologies.

IV. RESULTS

The segmentation accuracy obtained with the proposed approach in the scenarios with phantoms and real datasets is presented in Table II. It can be seen that the proposed method reaches high average DSC values of 0.957 ± 0.014 and 0.938 ± 0.015 , in each scenario, respectively.

The good quantitative results can also be confirmed visually. More precisely, it was noted that almost all vessels are correctly segmented in all cases, while only a few small vessels are lost during the segmentation process. The left side of Figure 4 shows 3D representations of the binary ground-truth and the segmentation obtained with the proposed method applied to the 4D ASL MRA dataset of subject 6. The blue circles indicate regions where the proposed segmentation method missed some small vessels. The right side of Figure 4 shows the maximum intensity projection of the 4D ASL MRA dataset of subject 6, with the ground-truth and resulting segmentations overlaid to complement the 3D visualization of the results.

Table III shows the average absolute error (AAE) for each estimated blood flow parameter ($A(v)$, δ_t , s , and p) in the

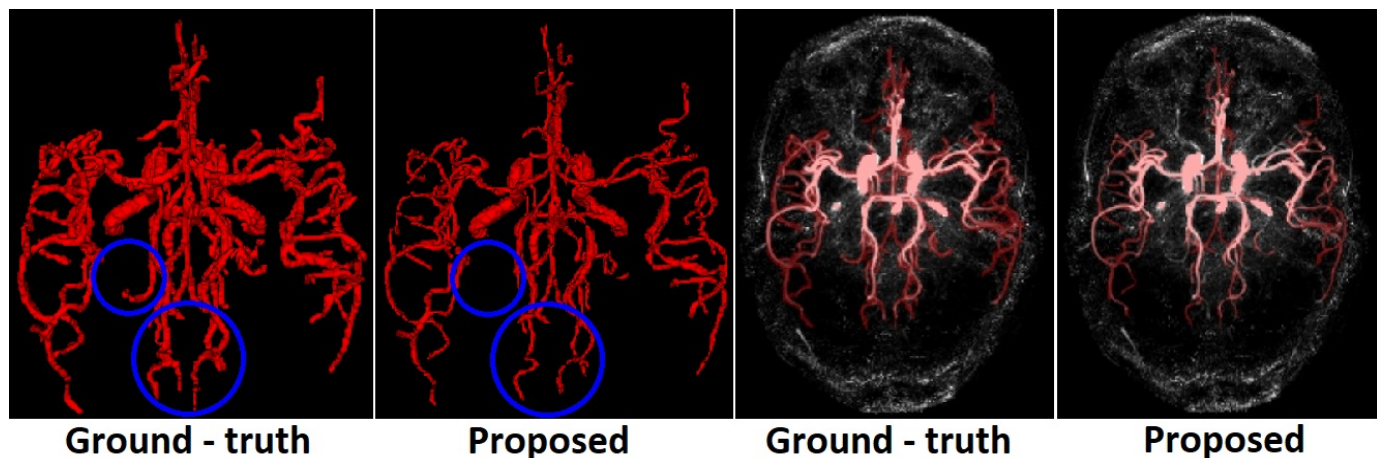


Fig. 4. Binary ground-truth and segmentation obtained with the proposed method using real 4D ASL MRA datasets of subject 6, presented as 3D representations (left) and overlaid on top of the maximum intensity projection of the 4D ASL MRA dataset (right). The circles in blue indicate areas where small vessels were not correctly identified.

Subject	DSC phantoms	DSC real
1	0.972	0.936
2	0.950	0.922
3	0.973	0.919
4	0.948	0.949
5	0.941	0.938
6	0.936	0.957
7	0.939	0.917
8	0.952	0.967
9	0.943	0.948
10	0.964	0.941
11	0.968	0.919
12	0.975	0.943
13	0.970	0.935
14	0.958	0.929
15	0.972	0.953
Average	0.957	0.938
SD	0.014	0.015

TABLE II
DICE SIMILARITY COEFFICIENT (DSC) ACCURACY VALUES AND STANDARD DEVIATION (SD) FOR THE PROPOSED SEGMENTATION METHOD, USING PHANTOMS AND REAL DATASETS.

phantoms scenario, before and after the blood flow parameter refinement step, respectively. The ANOVA analysis and post-hoc Tukey test indicate that the AAE between the estimated values and their corresponding ground-truth for $A(v)$ and δ_t is significantly improved after the refinement step. On the other hand, the AAEs of s and p are only improved by 1.81% and 8.22% after the refinement step, respectively. The resulting p-values for $A(v)$, δ_t , s , and p are 0.01, 0.01, 0.73, and 0.07, respectively.

On average, the refinement step seems to reduce the AAE of the estimated blood flow parameters. Nevertheless, some exceptions are present for each parameter. In case of $A(v)$, the refinement step increased the AAE for subjects 3 and 12. The same effect was observed for δ_t , in subject 10; for s in subjects 1, 6, 11, 12, and 15; and for p in subjects 1, 3, 7, 9, 10, and 12.

Figure 5 contains 3D representations of all estimated blood flow parameters in the 4D ASL MRA dataset of subject 6. A visual improvement can be noted in all cases, comparing

the top and middle row, as the refinement step generates images with a smoother appearance. The absolute differences between the uncorrected and corrected blood flow parameter images are shown in the bottom row.

Table IV shows the results of the qualitative evaluation of the estimated blood flow parameters $A(v)$ and δ_t in real datasets. The visualizations of the refined blood flow parameters were judged superior or equal to the raw hemodynamic parameters in all cases. It can also be noted that significantly higher scores are assigned to sets of images of both blood flow parameters after the refinement step, according to the ANOVA and post-hoc Tukey test. The p-values for $A(v)$ and δ_t are lower than 0.001 in both cases.

Finally, Figure 6 shows the result of applying the segmentation-based blood flow parameter refinement method to 4D ASL MRA datasets of patients with a stenosis in the carotid arteries. The 3D representations correspond to estimations of the transit time δ_t , with and without refinement, for the two patients. It can be noted that one side of the cerebrovascular system of patient 1 presents longer transit times compared to the corresponding vessel territory in the contralateral hemisphere, which corresponds well with the diagnosis of 80% occlusion of the LICA and 20% occlusion of the RICA for this patient. Consequently, the signal of labeled blood could not be imaged as far in one region. Overall, the effects of the presence of stenosis can be clearly seen in the refined blood flow parameter image while this effect is less obvious in the unrefined parameter image. For patient 2, there is no evident difference between the two sides of the cerebrovascular system, which is also in line with the clinical diagnosis of a bilateral stenosis of 30%. Again, the refined blood flow parameter visualization is less noisy compared to the unrefined blood flow parameter visualization, highlighting the utility of the proposed method in patients with a stenosis.

The correlation coefficient was also calculated for the blood flow parameter estimations using 4D ASL MRA datasets of patients with a stenosis in the carotid arteries. The correlation coefficient values for the relative blood volume A , transit time

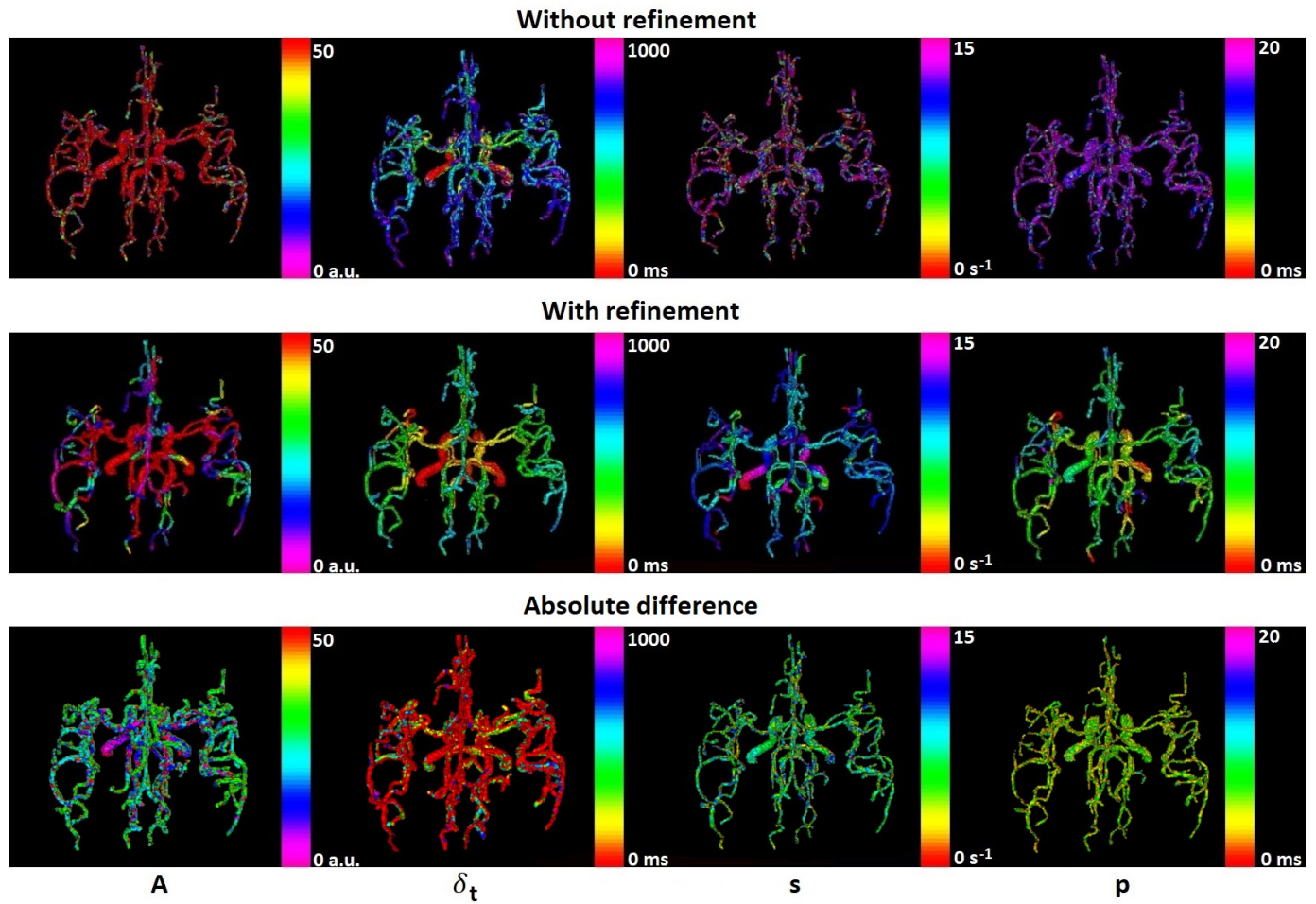


Fig. 5. 3D representations of the estimated blood flow parameters: relative blood volume A , transit time δ_t , blood dispersion sharpness s , and time-to-peak p along the vessels. The top row shows the hemodynamic parameters obtained from real 4D ASL MRA datasets without refinement, the middle row shows them after the refinement step, and the bottom row shows the absolute difference between both results.

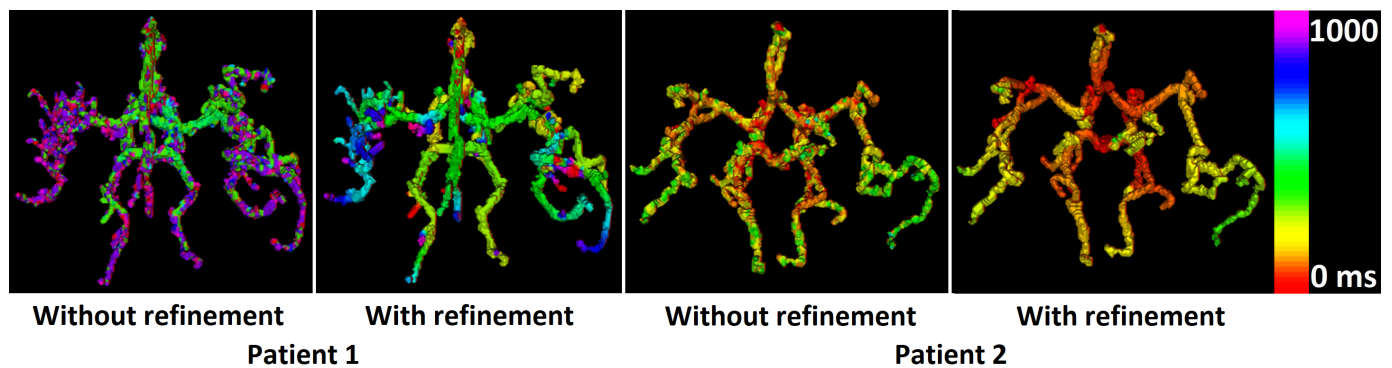


Fig. 6. 3D representations of the estimated transit time δ_t along the vessels for patients 1 and 2, without and with the refinement step. Both patients were diagnosed with carotid stenosis.

Subject	$A(v)$ (a.u.)	$A(v)$ refined (a.u.)	δ_t (ms)	δ_t refined (ms)	s (s^{-1})	s refined (s^{-1})	p (ms)	p refined (ms)
1	6.06	5.94	79.51	57.85	2.51	3.32	2.71	2.80
2	5.85	5.11	71.79	65.78	3.12	2.97	3.27	2.39
3	6.32	6.37	51.72	50.89	3.50	3.39	2.97	3.17
4	7.09	5.52	68.55	45.41	3.57	3.48	3.20	2.61
5	7.14	4.40	62.16	52.50	3.59	3.47	3.34	2.55
6	7.90	6.27	80.91	59.02	3.18	3.19	2.91	2.09
7	5.63	4.70	106.35	51.97	2.88	2.82	2.96	3.04
8	5.86	4.95	51.44	43.79	3.83	3.49	2.94	2.73
9	6.96	6.33	58.69	56.42	3.50	3.13	2.87	2.99
10	5.48	4.33	44.09	66.74	3.73	3.45	3.00	3.06
11	5.75	5.67	92.95	75.33	1.72	2.31	2.42	2.25
12	4.52	5.21	114.85	75.37	2.71	2.99	2.54	3.18
13	6.50	4.99	117.60	69.37	3.34	2.49	3.84	3.26
14	6.65	5.61	91.57	52.27	3.14	2.88	3.46	3.24
15	5.42	5.24	88.67	71.89	2.64	2.68	3.22	2.56
Average	6.21	5.37	78.72	59.64	3.13	3.07	3.04	2.79
SD	0.85	0.66	23.10	10.47	0.56	0.38	0.36	0.38

TABLE III

AVERAGE ABSOLUTE ERROR AND STANDARD DEVIATION (SD) OF EACH ESTIMATED BLOOD FLOW PARAMETER ($A(v)$, δ_t , s , AND p) IN THE PHANTOMS SCENARIO, BEFORE AND AFTER THE BLOOD FLOW PARAMETER REFINEMENT STEP. SIGNIFICANT DIFFERENCES ARE INDICATED IN BOLD.

Sub.	$A(v)$ (a.u.)	$A(v)$ ref. (a.u.)	δ_t (ms)	δ_t ref. (ms)
1	1	6	4	6
2	2	4	5	6
3	2	3	4	4
4	3	4	5	6
5	3	5	2	6
6	2	6	3	5
7	3	4	2	5
8	3	5	5	6
9	3	5	3	4
10	4	5	3	5
11	1	5	2	6
12	3	4	5	5
13	1	5	2	5
14	3	5	3	4
15	3	4	1	5
Avg.	2.47	4.67	3.27	5.20
SD	0.92	0.82	1.34	0.78

TABLE IV

GRADE ASSIGNED TO EACH ESTIMATED BLOOD FLOW PARAMETER ($A(v)$, δ_t) IN THE REAL DATASETS SCENARIO, BEFORE AND AFTER BLOOD FLOW PARAMETER REFINEMENT. SIGNIFICANT DIFFERENCES ARE IN BOLD.

δ_t , sharpness s , and time-to-peak p were 0.706, 0.787, 0.649, and 0.591 for patient 1, and 0.755, 0.832, 0.635, and 0.674 for patient 2, respectively. These values are within the ranges calculated for healthy subjects, showing that the refinement assumptions can also be applied to datasets of patients with this cerebrovascular disorder.

V. DISCUSSION

This work presented a novel method for the segmentation-based refinement of hemodynamic parameters extracted from 4D ASL MRA datasets. 4D ASL MRA is an imaging modality that can capture morphological and hemodynamic data of the cerebrovascular system at the same time, with high spatio-temporal resolution, when compared to other modalities [2]. The proposed method uses the morphological information contained in the segmented cerebrovascular system to refine the estimated blood flow parameter values, by considering their spatial dependency while the segmentation makes use of the hemodynamic information to improve the accuracy of the final vessel segmentation.

The results of the experiments shown in this paper suggest that the method generated accurate segmentations, reaching DSC values of 0.957 and 0.938 when using phantoms and real datasets, respectively. On the other hand, the results of this work indicate that the blood flow parameters estimated using the model proposed by Okell et al. [26] can be significantly improved by making use of the morphological information of the cerebrovascular system. In particular, the centerline of the resulting segmentation contains the most relevant blood flow information, which was used to model each blood flow parameter [8].

The quantitative evaluation using 15 4D ASL MRA phantom datasets, showed that a significant improvement can be achieved for the estimation of blood flow parameters $A(v)$ and δ_t , and a non-significant improvement in case of s and p . Some individual exceptions were observed, where the refinement step increased the AAE. One of the main reasons for these exceptions is that the estimated blood flow parameters contained a considerable amount of outliers, which could not be handled by the regression method used. In this case, an outlier removal algorithm could improve the refinement step. Additionally, the qualitative evaluation of the proposed method showed that the refined blood flow parameter images are more physiologically reasonable than the non-refined ones.

It should be noted that even though the 4D ASL MRA phantoms were generated with the same mathematical model used to estimate the blood flow parameter values (see Equation 1), there are many factors that can potentially contribute to errors in the results and make the phantom datasets suitable for quantitative comparison. More specifically, these factors include the presence of partial volume effects and homomorphic noise [36], the accuracy of the cerebrovascular segmentation that is used for refinement of the blood flow parameter estimations, and the algorithm used to fit the mathematical model to the observed vascular signal.

The method described in this work can support the translation of 4D ASL MRA from research to clinical practice, as a non-invasive alternative to DSA to study the cerebrovascular system, by simultaneously providing morphological and hemo-

dynamic information. To the best of our knowledge, this is the first method that refines the estimated blood flow parameters along the segmented vascular tree so that more physiologically reasonable measurements and visualizations can be provided to the user.

Considering that 4D ASL MRA is a non-invasive modality, this method can potentially be used to study healthy subjects and define criteria of normality in terms of vascular morphology and hemodynamics and to image and follow-up with patients after treatment. Additionally, given its modular design, the proposed method could also be adapted to process other 4D angiography datasets, such as CTA or other 4D MRA image sequences. This adaptation would essentially require the use of a different mathematical model to describe the signal generated by the contrast agent used in the selected modality.

Regarding the limitations of the proposed method, it can be argued that 4D ASL MRA typically requires reasonably high arterial velocities. Consequently, it might not be suitable for visualization of vessels with severe stenoses. Although it is true that some vessels might not be displayed properly, the effects of stenoses can be noticed by the presence of longer transit times and absence of signal in vascular regions with larger transit times than the acquisition time (see Figure 6).

It should also be noted that the datasets of patients with a stenosis used in the experiments of this work were acquired with a slightly different labeling strategy than the datasets of healthy subjects, PASL and PCASL, respectively. Consequently, further improvement of the method would include accounting for slight differences between both strategies. In particular, Equation 1 could be modified to consider the additional relaxation that the labeled blood signal of PASL experiences between the start and end of the bolus [40].

Additionally, the refinement step corrects the parameters assuming a forward flow direction, which might not hold true in some cases, such as in aneurysms that present turbulent flow. In order to highlight these anomalies, it would be possible to generate an image indicating the difference between the refined parameters and the original estimated value (see Figure 5).

Additional improvement to the refinement step could be achieved by implementing alternative skeletonization algorithms of the segmentation of the brain vascular system. However, a visual analysis of our results confirmed that the skeletons were not disconnected and well centered in the middle of the vascular system so that the improvement applying other centerline extraction methods might be rather minor. Nevertheless, recent skeletonization algorithms can achieve faster processing times by using parallel computing [41].

The refinement step used in this work basically assumes the continuity of the hemodynamic parameters along the cerebrovascular system. Further improvement might be achieved by adding more physical and physiological constraints. However, this work has purposefully not included any tight constraints such as Murray's Law or the conservation of mass of blood for the blood flow parameter refinement but proposes an assumption-light data-driven regression approach. The reason for doing so is that cerebrovascular diseases such as stenoses or moyamoya disease may be associated with a violation of these assumptions, while the purely data-driven approach suggested

in this work is theoretically more robust in these cases. Within this context, it might also be beneficial to use non-parametric regression methods in case of severe pathologies, such as a b-spline interpolation.

Finally, it is important to mention that other imaging modalities can also be used to measure blood flow parameters in the brain. In particular, 4D flow MRI can acquire images of the whole cerebrovascular system, with similar resolution to 4D ASL MRA, in reasonable acquisition times of approximately 9 minutes [15], [16]. Within this context, it would be interesting to compare and evaluate both image sequences together in healthy subjects and patients with cerebrovascular diseases as similar blood flow parameters can be calculated from both sequences. In contrast to 4D ASL MRA, which displays the passage of magnetically labeled blood, 4D flow MRI measures the flow velocity directly. Thus, both imaging modalities might really complement each other. Unfortunately, 4D flow MRI datasets were not available for the subjects and patients in this study so that this question needs to be addressed in detail in future studies. Apart from this, it should also be mentioned that the segmentation-based blood flow parameter refinement could also be applied to the velocity measurements in single frames of 4D flow MRI datasets.

VI. CONCLUSION

The present paper describes a new segmentation-based method to refine hemodynamic parameter maps computed from 4D ASL MRA datasets. The cerebrovascular segmentation is used to refine relevant blood flow parameter data contained in the centerline of the vessels, which can improve the accuracy of the estimated parameter value, and its visual representation, by considering its spatial dependency. This method should allow clinicians and researchers to analyze and study the cerebrovascular system non-invasively, thus, avoiding the costs and risks associated to ionizing radiation exposure and contrast agent administration.

ACKNOWLEDGEMENTS

This work was supported by Alberta Innovates (AIHS), Hotchkiss Brain Institute (HBI), and Natural Sciences and Engineering Research Council of Canada (NSERC). Dr. Nils D. Forkert is funded by Canada Research Chairs. Dr. Alexandre X. Falcão thanks CNPq 303808/2018-7 and FAPESP 2014/12236-1.

REFERENCES

- [1] J. Liu, X.-J. Jia, Y.-J. Wang, M. Zhang, T. Zhang, and H.-D. Zhou, "Digital subtraction angiography imaging characteristics of patients with extra-intracranial atherosclerosis and its relationship to stroke," *Cell biochemistry and biophysics*, vol. 69, no. 3, pp. 599–604, 2014.
- [2] X. Bi, P. Weale, P. Schmitt, S. Zuehlsdorff, and R. Jerecic, "Non-contrast-enhanced four-dimensional (4D) intracranial MR angiography: A feasibility study," *Magnetic resonance in medicine*, vol. 63, no. 3, pp. 835–841, 2010.
- [3] R. Thiex, A. Norbash, and K. Frerichs, "The safety of dedicated-team catheter-based diagnostic cerebral angiography in the era of advanced noninvasive imaging," *American journal of neuroradiology*, vol. 31, no. 2, pp. 230–234, 2010.

- [4] J. J. Connors III, D. Sacks, A. J. Furlan, W. R. Selman, E. J. Russell, P. E. Stieg, and M. N. Hadley, "Training, competency, and credentialing standards for diagnostic cervicocerebral angiography, carotid stenting, and cerebrovascular intervention: A joint statement from the American Academy of Neurology, American Association of Neurological Surgeons, American Society of Interventional and Therapeutic Radiology, American Society of Neuroradiology, Congress of Neurological Surgeons, AANS/CNS Cerebrovascular Section, and the Society of Interventional Radiology," *Radiology*, vol. 234, no. 1, pp. 26–34, 2005.
- [5] W. A. Willinek, D. R. Hadizadeh, M. von Falkenhausen, H. Urbach, R. Hoogeveen, H. H. Schild, and J. Gieseke, "4D time-resolved MR angiography with keyhole (4D-TRAK): More than 60 times accelerated MRA using a combination of CENTRA, keyhole, and SENSE at 3.0 T," *Journal of Magnetic Resonance Imaging*, vol. 27, no. 6, pp. 1455–1460, 2008.
- [6] F. R. Korosec, R. Frayne, T. M. Grist, and C. A. Mistretta, "Time-resolved contrast-enhanced 3D MR angiography," *Magnetic Resonance in Medicine*, vol. 36, no. 3, pp. 345–351, 1996.
- [7] G. Laub and R. Kroeker, "Syngo twist for dynamic time-resolved MR angiography," *Magnetom Flash*, vol. 3, pp. 92–95, 2006.
- [8] N. D. Forkert, J. Fiehler, T. Illies, D. P. Möller, H. Handels, and D. Säring, "4D blood flow visualization fusing 3D and 4D MRA image sequences," *Journal of magnetic resonance imaging*, vol. 36, no. 2, pp. 443–453, 2012.
- [9] T. Illies, N. Forkert, T. Ries, J. Regelsberger, and J. Fiehler, "Classification of cerebral arteriovenous malformations and intranidal flow patterns by color-encoded 4d-hybrid-mra," *American journal of neuroradiology*, vol. 34, no. 1, pp. 46–53, 2013.
- [10] W. Williamson, A. J. Lewandowski, N. D. Forkert, L. Griffanti, T. W. Okell, J. Betts, H. Boardman, T. Siepmann, D. McKean, O. Huckstep *et al.*, "Association of cardiovascular risk factors with MRI indices of cerebrovascular structure and function and white matter hyperintensities in young adults," *Journal of the American Medical Association*, vol. 320, no. 7, pp. 665–673, 2018.
- [11] D. Lesage, E. D. Angelini, I. Bloch, and G. Funka-Lea, "A review of 3D vessel lumen segmentation techniques: Models, features and extraction schemes," *Medical image analysis*, vol. 13, no. 6, pp. 819–845, 2009.
- [12] T. Deschamps, P. Schwartz, D. Trebotich, P. Colella, D. Saloner, and R. Malladi, "Vessel segmentation and blood flow simulation using level-sets and embedded boundary methods," in *International congress series*, vol. 1268. Elsevier, 2004, pp. 75–80.
- [13] J. Mordang, M. Oei, R. van den Boom, E. Smit, M. Prokop, B. van Ginneken, and R. Manniesing, "A pattern recognition framework for vessel segmentation in 4D CT of the brain," in *SPIE medical imaging*. International Society for Optics and Photonics, 2013, pp. 866919–866919.
- [14] K. A. Patwardhan, Y. Yu, S. Gupta, A. Dentinger, and D. Mills, "4D vessel segmentation and tracking in ultrasound," in *Image Processing (ICIP), 2012 19th IEEE International Conference on*. IEEE, 2012, pp. 2317–2320.
- [15] T. Dunås, M. Holmgren, A. Wåhlin, J. Malm, and A. Eklund, "Accuracy of blood flow assessment in cerebral arteries with 4D flow MRI: Evaluation with three segmentation methods," *Journal of magnetic resonance imaging*, 2019.
- [16] E. Schrauben, A. Wåhlin, K. Ambarki, E. Spaak, J. Malm, O. Wieben, and A. Eklund, "Fast 4D flow MRI intracranial segmentation and quantification in tortuous arteries," *Journal of magnetic resonance imaging*, vol. 42, no. 5, pp. 1458–1464, 2015.
- [17] R. Phellan, T. Linder, M. Helle, A. X. Falcão, and N. D. Forkert, "Robust cerebrovascular segmentation in 4D ASL MRA images," in *IEEE 15th international symposium on biomedical imaging (ISBI 2018)*. IEEE, 2018, pp. 1348–1351.
- [18] W. Dai, D. Garcia, C. De Bazelaire, and D. C. Alsop, "Continuous flow-driven inversion for arterial spin labeling using pulsed radio frequency and gradient fields," *Magnetic resonance in medicine*, vol. 60, no. 6, pp. 1488–1497, 2008.
- [19] E. C. Wong, R. B. Buxton, and L. R. Frank, "Implementation of quantitative perfusion imaging techniques for functional brain mapping using pulsed arterial spin labeling," *Nuclear magnetic resonance in biomedicine*, vol. 10, no. 4-5, pp. 237–249, 1997.
- [20] P. Coupé, P. Yger, S. Prima, P. Hellier, C. Kervrann, and C. Barillot, "An optimized blockwise nonlocal means denoising filter for 3D magnetic resonance images," *IEEE transactions on medical imaging*, vol. 27, no. 4, pp. 425–441, 2008.
- [21] M. Erdt, M. Raspe, and M. Sühling, "Automatic hepatic vessel segmentation using graphics hardware," in *Medical imaging and augmented reality*. Springer, 2008, pp. 403–412.
- [22] R. Phellan and N. D. Forkert, "Comparison of vessel enhancement algorithms applied to time-of-flight MRA images for cerebrovascular segmentation," *Medical physics*, vol. 44, no. 11, pp. 5901–5915, 2017.
- [23] S. Lankton and A. Tannenbaum, "Localizing region-based active contours," *IEEE transactions on image processing*, vol. 17, no. 11, pp. 2029–2039, 2008.
- [24] A. X. Falcão, J. Stolfi, and R. A. Lotufo, "The image foresting transform: Theory, algorithms, and applications," *IEEE transactions on pattern analysis and machine intelligence*, vol. 26, no. 1, pp. 19–29, 2004.
- [25] N. D. Forkert, J. Fiehler, T. Ries, T. Illies, D. Möller, H. Handels, and D. Säring, "Reference-based linear curve fitting for bolus arrival time estimation in 4d mra and mr perfusion-weighted image sequences," *Magnetic resonance in medicine*, vol. 65, no. 1, pp. 289–294, 2011.
- [26] T. W. Okell, M. A. Chappell, U. G. Schulz, and P. Jezard, "A kinetic model for vessel-encoded dynamic angiography with arterial spin labeling," *Magnetic resonance in medicine*, vol. 68, no. 3, pp. 969–979, 2012.
- [27] H. Lu, C. Clingman, X. Golay, and P. van Zijl, "Determining the longitudinal relaxation time (T1) of blood at 3.0 Tesla," *Magnetic resonance in medicine*, vol. 52, no. 3, pp. 679–682, 2004.
- [28] G. C. Ruppert, G. Chiachia, F. P. Bergo, F. O. Favretto, C. L. Yasuda, A. Rocha, and A. X. Falcão, "Medical image registration based on watershed transform from greyscale marker and multi-scale parameter search," *Computer methods in biomechanics and biomedical engineering: Imaging and visualization*, pp. 1–19, 2015.
- [29] H. Homann, "Implementation of a 3D thinning algorithm," *Insight journal*, vol. 421, 2007.
- [30] T.-C. Lee, R. L. Kashyap, and C.-N. Chu, "Building skeleton models via 3-D medial surface axis thinning algorithms," *Graphical models and image processing*, vol. 56, no. 6, pp. 462–478, 1994.
- [31] D. M. Corey, W. P. Dunlap, and M. J. Burke, "Averaging correlations: Expected values and bias in combined Pearson r s and Fisher's z transformations," *The journal of general psychology*, vol. 125, no. 3, pp. 245–261, 1998.
- [32] R. Phellan, T. Lindner, M. Helle, A. X. Falcão, T. W. Okell, and N. D. Forkert, "A methodology for generating four-dimensional arterial spin labeling MR angiography virtual phantoms," *Medical image analysis*, vol. 56, pp. 184–192, 2019.
- [33] N. D. Forkert, A. Schmidt-Richberg, J. Fiehler, T. Illies, D. Möller, D. Säring, H. Handels, and J. Ehrhardt, "3D cerebrovascular segmentation combining fuzzy vessel enhancement and level-sets with anisotropic energy weights," *Magnetic resonance imaging*, vol. 31, no. 2, pp. 262–271, 2013.
- [34] M. E. MacDonald and R. Frayne, "Phase contrast MR imaging measurements of blood flow in healthy human cerebral vessel segments," *Physiological measurement*, vol. 36, no. 7, p. 1517, 2015.
- [35] L. Zarrinkoob, K. Ambarki, A. Wåhlin, R. Birgander, A. Eklund, and J. Malm, "Blood flow distribution in cerebral arteries," *Journal of cerebral blood flow and metabolism*, vol. 35, no. 4, pp. 648–654, 2015.
- [36] S. Aja-Fernández, T. Pie, G. Vegas-Sánchez-Ferrero *et al.*, "Spatially variant noise estimation in MRI: A homomorphic approach," *Medical image analysis*, vol. 20, no. 1, pp. 184–197, 2015.
- [37] L. R. Dice, "Measures of the amount of ecologic association between species," *Ecology*, vol. 26, no. 3, pp. 297–302, 1945.
- [38] S. Klein, M. Staring, K. Murphy, M. A. Viergever, and J. P. Pluim, "Elastix: A toolbox for intensity-based medical image registration," *IEEE transactions on medical imaging*, vol. 29, no. 1, pp. 196–205, 2010.
- [39] S. D. Shpilfoygel, R. A. Close, D. J. Valentino, and G. R. Duckwiler, "X-ray videodensitometric methods for blood flow and velocity measurement: A critical review of literature," *Medical physics*, vol. 27, no. 9, pp. 2008–2023, 2000.
- [40] R. B. Buxton, L. R. Frank, E. C. Wong, B. Siewert, S. Warach, and R. R. Edelman, "A general kinetic model for quantitative perfusion imaging with arterial spin labeling," *Magnetic resonance in medicine*, vol. 40, no. 3, pp. 383–396, 1998.
- [41] P. K. Saha, G. Borgefors, and G. S. di Baja, "A survey on skeletonization algorithms and their applications," *Pattern recognition letters*, vol. 76, pp. 3–12, 2016.